




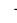






K-shell photoionisation of O⁴⁺ and O⁵⁺ ions : experiment and theory

B. M. McLaughlin^{1,2} , J.-M. Bizau^{3,4} , D. Cubaynes^{3,4} , S. Guilbaud³ , S. Douix⁴ ,
M. M. Al Shorman⁵ , M. O. A. El Ghazaly⁶ , I. Sakho⁷   and M. F. Gharaibeh⁸ 

¹Centre for Theoretical Atomic and Molecular Physics (CTAMOP), School of Mathematics and Physics,
Queen's University Belfast, Belfast BT7 1NN, Northern Ireland, UK

²Institute for Theoretical Atomic and Molecular Physics (ITAMP)

Harvard Smithsonian Center for Astrophysics, MS-14, Cambridge, MA 02138, USA

³Institut des Sciences Moléculaires d'Orsay (ISMO), CNRS UMR 8214,
Univ. Paris-Sud, Université Paris-Saclay, F-91405 Orsay cedex, France

⁴Synchrotron SOLEIL - L'Orme des Merisiers, Saint-Aubin - BP 48 91192 Gif-sur-Yvette cedex, France

⁵Applied Physics Department, Faculty of Science, Tafila Technical University, Tafila 66110, Jordan

⁶Astrophysics and Space Sciences Section, Jet Propulsion Laboratory, Caltech, Pasadena, CA 91109, USA

⁷Department of Physics, UFR of Sciences and Technologies, University Assane Seck of Ziguinchor, Ziguinchor, Senegal

⁸Department of Mathematics, Statistics and Physics, P.O. Box 2713, Qatar University, Doha, Qatar

Accepted –; Received 9 March 2022; in original form September, 7, 2016

ABSTRACT

Absolute cross sections for the *K*-shell photoionisation of Be-like (O⁴⁺) and Li-like (O⁵⁺) atomic oxygen ions were measured for the first time (in their respective *K*-shell regions) by employing the ion-photon merged-beam technique at the SOLEIL synchrotron-radiation facility in Saint-Aubin, France. High-resolution spectroscopy with $E/\Delta E \approx 3200$ (≈ 170 meV, FWHM) was achieved with photon energy from 550 eV up to 670 eV. Rich resonance structure observed in the experimental spectra is analysed using the R-matrix with pseudo-states (RMPS) method. Results are also compared with the screening constant by unit nuclear charge (SCUNC) calculations. We characterise and identify the strong $1s \rightarrow 2p$ resonances for both ions and the weaker $1s \rightarrow np$ resonances ($n \geq 3$) observed in the *K*-shell spectra of O⁴⁺.

Key words: atomic data – atomic processes – photoionisation

1 INTRODUCTION

The launch of the satellite Astro-H (re-named Hitomi) on February 17, 2016, was expected to provide x-ray spectra of unprecedented quality and would have required a wealth of atomic and molecular data on a range of collision processes to assist with the analysis of spectra from a variety of astrophysical objects. The subsequent break-up on March 28, 2016 of Hitomi now leaves a void in observational x-ray spectroscopy. In the intervening period before the launch of

the next x-ray satellite mission, ground-based x-ray experiments along with theoretical cross sections will continue to be benchmarked against one and other, in order to extend our database of knowledge on astrophysical important ions of carbon, nitrogen and oxygen.

Measurements of cross sections for photoionisation of atoms and ions are essential data for testing theoretical methods in fundamental atomic physics (Berkowitz 1979; West 2001; Kjeldsen et al. 2002; Müller 2015) and for modeling of many physical systems, for example terrestrial plasmas, the upper atmosphere, and a broad range of astrophysical objects (quasar stellar objects, the atmosphere of hot stars, proto-planetary nebulae, H II regions, novae, and supernovae) (Lee et al. 2001; Blustin et al. 2002, 2003; Kaastra et al. 2002, 2004; Juett et al. 2004; Pinto et al. 2013, 2014; Nicastro et al. 2016a,b).

X-ray spectroscopy of highly ionised atomic oxygen is used to probe the hot gaseous halo of the Milky Way (Nicastro et al. 2016c; Miller & Bergman 2015; Gupta et al. 2012,

* bmclaughlin899@btinternet.com :corresponding author

† jean-marc.bizau@u-psud.fr

‡ denis.cubaynes@u-psud.fr

§ segolene.guilbaud@u-psud.fr

¶ suzie.douix@synchrotron-soleil.fr

|| mmaa1984@yahoo.com

** mael46@gmail.com

†† animafatima_sakho@yahoo.fr

‡‡ mgharaibeh@qu.edu.qa: prior address, Department of Physics,
Jordan University of Science and Technology, Irbid 22110, Jordan

2014). Multiply ionisation stages of C, N, O, Ne and Fe have been observed in the ionised outflow in the planetary nebulae NGC 4051, and measured with the satellite *XMM-Newton* (Ogle et al. 2004; Pinto et al. 2013) in the soft-x-ray region. Low ionised stages of C, N and O have also been used in the modelling of x-ray emission from OB supergiants (Cassinelli et al. 1981). Multiply ionisation stages of O and Fe are also seen in the *XMM-Newton* spectra from the Seyfert galaxy NGC 3783, including UV imaging, x-ray and UV light curves, the 0.2 – 10 keV x-ray continuum, the iron *K* - emission line, and high-resolution spectroscopy in the modelling of the soft x-ray warm absorber (Blustin et al. 2002, 2003; Krongold et al. 2003; Mendoza et al. 2012; Gorczyca et al. 2013; Gattuzz et al. 2013a, 2014).

Limited wavelength observations for x-ray transitions were recently made on atomic oxygen, neon and magnesium and their ions with the High Energy Transmission Grating (HETG) on board the *Chandra* satellite (Liao et al. 2013). Strong absorption *K*-shell lines of atomic oxygen, in its various forms of ionisation have been observed by the *XMM-Newton* satellite in the interstellar medium, through x-ray spectroscopy of low-mass x-ray binaries (Pinto et al. 2013). The *Chandra* and *XMM-Newton* satellite observations may be used to identify absorption features in astrophysical sources, such as AGN and x-ray binaries and for assistance in benchmarking theoretical and experimental work (McLaughlin et al. 2013a,b; Gorczyca et al. 2013; Gattuzz et al. 2013a,b, 2014; McLaughlin et al. 2014; Bizau et al. 2015).

To our knowledge previous experimental and observational x-ray lines on Be-like and Li-like atomic oxygen ions are limited to the $1s \rightarrow np$ regions (where $n=2, 3, 4$, and 5), i.e., the K_α , K_β , K_γ and K_δ lines, in the vicinity of the *K*-shell region (Nicolosi & Tondello 1997; Bruch et al. 1979, 1987; Hoffmann et al. 1990, 1991; Behar et al. 2003; Schmidt et al. 2004; Gu et al. 2005; Lee et al. 2001; Kaastra et al. 2002, 2004; Yao et al. 2009; Mendoza et al. 2012; Ramírez 2013; Liao et al. 2013; Pinto et al. 2013, 2014; Cabot et al. 2013; Nicastro et al. 2016a,b). Prior to the present *K*-shell investigations at the SOLEIL radiation facility on photoionisation cross sections and Auger resonance states along the atomic oxygen iso-nuclear sequence, few experiments have been devoted to the study of *K*-shell photoionisation of oxygen ions. Nicolosi and Tondello (Nicolosi & Tondello 1997) observed satellite lines of He-like and Li-like laser produced plasmas of Be, B, C, N and O. Auger spectra of core-excited oxygen ions emitted in the collision of fast oxygen-ion beams with gas targets and foils were measured by Bruch and co-workers (Bruch et al. 1979, 1987). Hoffmann and co-workers (Hoffmann et al. 1990, 1991) measured Auger resonance energies in electron-impact ionisation studies of Be-like and Li-like ions. *K*-shell x-ray lines from inner-shell excited and ionised ions of oxygen, were observed using the Lawrence Livermore National Laboratory EBIT from O^{2+} to O^{5+} (Schmidt et al. 2004; Gu et al. 2005).

For the oxygen iso-nuclear sequence theoretical data are available for the energies for *K*-shell Auger or radiative transitions. Resonance energies and line widths for Auger transitions in Be-like (Bruch et al. 1979) and Li-like atomic ions (Piangos & Nicolaides 1993) have been calculated using a variety of methods such as $1/Z$ perturbation theory (Murakami et al. 2002), multi-configuration Dirac Fock (MCDF) (Bruch

et al. 1979; Chen 1985, 1986; Chen et al. 2006), the saddle-point-method (SPM) with R-matrix (Davis & Chung 1985, 1989) and complex-coordinate rotation methods (Zhang & Yeager 2012b,a). We note that Moore (Moore 1993) made an assessment of the energy levels of Carbon, Nitrogen and Oxygen atoms and their ions. Chen and co-workers calculated Auger and radiative decay of $1s$ -vacancy states in the Be iso-electronic sequence using the MCDF approach (Chen 1985, 1986; Chen & Crasemann 1987b). Zhang and Yeager (Zhang & Yeager 2012b) used the SPM with rotation (Davis & Chung 1985; Bingcong & Wensheng 2000) to calculate energy levels and Auger decay widths for the $1s2s^22p^1\ ^3P^o$ levels in Be-like system. The recent saddle-point with rotation calculations by Yeager and co-workers (Zhang & Yeager 2012b), for resonance energies and Auger decay rates, for the $1s2s^22p^1\ ^1P^o$ levels in Be-like carbon showed excellent agreement with previous measurements made at the Advanced Light Source (ALS) and R-matrix calculations (Scully et al. 2005).

In the case of Be-like and Li-like atomic oxygen systems, state-of-the-art *ab initio* photoionisation cross sections, resonance energies and decay rates for Auger inner-shell processes, were performed by Pradhan and co-workers (Pradhan 2000; Nahar et al. 2001; Pradhan et al. 2003) using the R-matrix method. Garcia and co-workers (Garcia et al. 2005) extended this work using the R-matrix optical potential method within an intermediate-coupling scheme (Burke 2011) to take account of Auger broadening of the resonances in the near *K*-edge region. Photoionisation from the ground state, along the oxygen iso-nuclear sequence was investigated, in the photon energy region of the *K*-edge for both Be-like and Li-like atomic oxygen ions.

In the present study we focus our attention on obtaining detailed spectra for Be-like $[O^{4+} \text{ (O V)}]$ and Li-like $[O^{5+} \text{ (O VI)}]$ atomic oxygen ions in the vicinity of the *K*-edge. The current work is the completion of photoionisation cross section measurements and theoretical studies along the atomic oxygen iso-nuclear sequence. Our previous studies on this sequence, focused on obtaining photoionisation cross sections for the O^+ and O^{2+} ions (Bizau et al. 2015) and the O^{3+} ion (McLaughlin et al. 2014), where differences of 0.5 eV in the positions of the K_α resonance lines with prior satellite observations were found. This will have major implications for astrophysical modelling.

2 EXPERIMENT

2.1 Ion production

The measurements were made using the MAIA (Multi-Analysis Ion Apparatus) merged-beam set-up on the PLEIADES photon beam line at SOLEIL, the French synchrotron radiation facility. The set-up and the experimental procedure have been described previously in detail (Bizau et al. 2016), and we will only give the characteristics of relevance for the present experiment. The oxygen ion beams are produced in a permanent magnet Electron Cyclotron Resonance Ion Source (ECRIS). Oxygen gas introduced in the ECRIS chamber is heated by a 12.6 GHz radio wave at a power of approximately 25W. A constant 4 kV bias is applied on the source to extract the ions. They are selected in mass/charge ratio by a dipole magnet before being

Table 1. Typical values for the experimental parameters involved in evaluating the absolute O^{4+} cross section measured at a photon energy of 554.25 eV.

| | |
|-------------|------------------------------------|
| S | 540 Hz |
| Noise | 150 Hz |
| ν | $5.4 \cdot 10^5 \text{ ms}^{-1}$ |
| Photon flux | $5.1 \cdot 10^{12} \text{ s}^{-1}$ |
| J | 50 nA |
| ϵ | 0.92 |
| F_{xy} | $5.9 \cdot 10^4 \text{ m}^{-1}$ |

collimated and merged with the photon beam in the 60 cm long interaction region. A second dipole magnet analyses the charge state of the ions after interaction with the photons. The parent ions are collected in a Faraday cup while the photo-ions (the ions which have increased in charge state by one in the interaction) are counted using channel plates.

2.2 Excitation source

The photon beam is the synchrotron radiation emitted by the Apple II undulator of the PLEIADES beam line. The light is monochromatised using a 600 l/mm high flux grating. In the energy range considered in this work, the spectral purity is achieved by the cut-off of the mirrors transmission and the use of a varied groove depth for the grating. The photon energy is determined using an ionisation chamber (Samson 1967). For this work, we used for calibration purpose an energy of $539.17 \pm 0.15 \text{ eV}$ for the $O_2 \text{ } 1s \rightarrow 3s\sigma$ transition as determined in Bizau et al. (2015). The photon energy is corrected for the Doppler shift produced by the two counter-propagating beams.

2.3 Experimental procedure

The absolute photoionisation cross sections σ are obtained at a given photon energy using the procedure previously described in Bizau et al. (2016) from the relation:

$$\sigma = \frac{Se^2\eta\nu q}{IJ\epsilon \int_0^L \frac{dz}{\Delta x \Delta y F(z)}}, \quad (1)$$

The photo-ions counting rate S is corrected from the spurious ion signal produced by collisional-ionisation processes using a chopper placed at the exit of the photon beam line. In equation (1), ν is the velocity in the interaction region of the target ions of charge state q , I is the current produced by the photons on a SXUV300 IRD photodiode of efficiency η calibrated at the Physikalisch-Technische Bundesanstalt (PTB) beam line at BESSY in Berlin, J is the current of incident ions, and ϵ the efficiency of the micro-channel plates. $\Delta x \Delta y F(z)$ is an effective beam area (with z the propagation axis of the two beams), where F is the two-dimensional form factor determined using three sets of xy slit scanners placed at each end and in the middle of the interaction region. The length L of the interaction region is fixed by applying -1 kV bias on the tube delimiting the interaction region. The bias discriminates the photo-ions produced inside and outside the tube due to their different velocity. Typical values of the parameters involved in equation (1), measured for O^{4+} target

ion at a photon energy of 554.25 eV, are given in Table 1. The cross sections accuracy is determined by the statistical fluctuations on the photo-ion and background counting rates, plus a systematic contribution resulting from the measurement of the different parameters in equation (1). The latter is estimated to be 15% and is dominated by the uncertainty on the determination of the photon flux and the form factor. Two modes are used for the acquisition of the cross sections. One with no bias applied to the interaction tube, allowing to determine with higher statistics and spectral resolution the relative cross sections, which are latter normalized on the absolute cross sections obtained in the second mode with the voltage applied to the interaction tube.

3 THEORY

3.1 SCUNC: Li-like and Be-like nitrogen

Previously we have used the Screening Constant by Unit Nuclear Charge (SCUNC) method in our theoretical work for O^{3+} (McLaughlin et al. 2014) to provide energies and Auger decay rates to complement our detailed *ab initio* calculations. The basic equations used to determine the resonance energy positions and the Auger widths are summarised here for completeness.

In the SCUNC formalism (Sakho 2011, 2012; Sakho et al. 2013), one has the total energy of the core-excited states given by,

$$E(N\ell n\ell'; {}^{2S+1}L^\pi) = -Z^2 \left[\frac{1}{N^2} + \frac{1}{n^2} (1 - \beta)^2 \right] \quad (2)$$

where $E(N\ell n\ell'; {}^{2S+1}L^\pi)$ is in Rydberg units. In this equation, the principal quantum numbers N and n are respectively for the inner and the outer electron of the He-like isoelectronic series. The β -parameters are screening constants by unit nuclear charge expanded in inverse powers of Z and are given by the expression,

$$\beta(N\ell n\ell'; {}^{2S+1}L^\pi) = \sum_{k=1}^q f_k \left(\frac{1}{Z} \right)^k \quad (3)$$

where $f_k(N\ell n\ell'; {}^{2S+1}L^\pi)$ are parameters to be evaluated empirically from previous experimental measurements. Similarly, one may get the Auger widths Γ in Rydbergs (1 Rydberg = 13.605698 eV) from the formula

$$\Gamma(\text{Ry}) = Z^2 \left[1 - \frac{f_1}{Z} \left(\frac{Z}{Z_0} - \frac{1}{Z^2} \frac{(Z - Z_0)}{Z_0^2} - \frac{1}{Z^3} \frac{(Z - Z_0)}{Z_0^3} \right) \right]^2 \quad (4)$$

The measurements of Müller and co-workers on Be-like boron and carbon, Li-like boron and carbon (Scully et al. 2005; Müller et al. 2009, 2010, 2014) were used to determine all the appropriate empirical parameters used in the present work.

3.2 R-matrix with pseudo-states

The *R*-matrix with pseudo-states (RMPS) method (Mitnik et al. 1999; Burke 2011) was used to calculate the inner-shell photoionisation cross sections for the atomic oxygen ions, O^{4+} and O^{5+} , in their respective *K*-shell energy regions. The *R*-matrix with pseudo-states method (Mitnik et al.

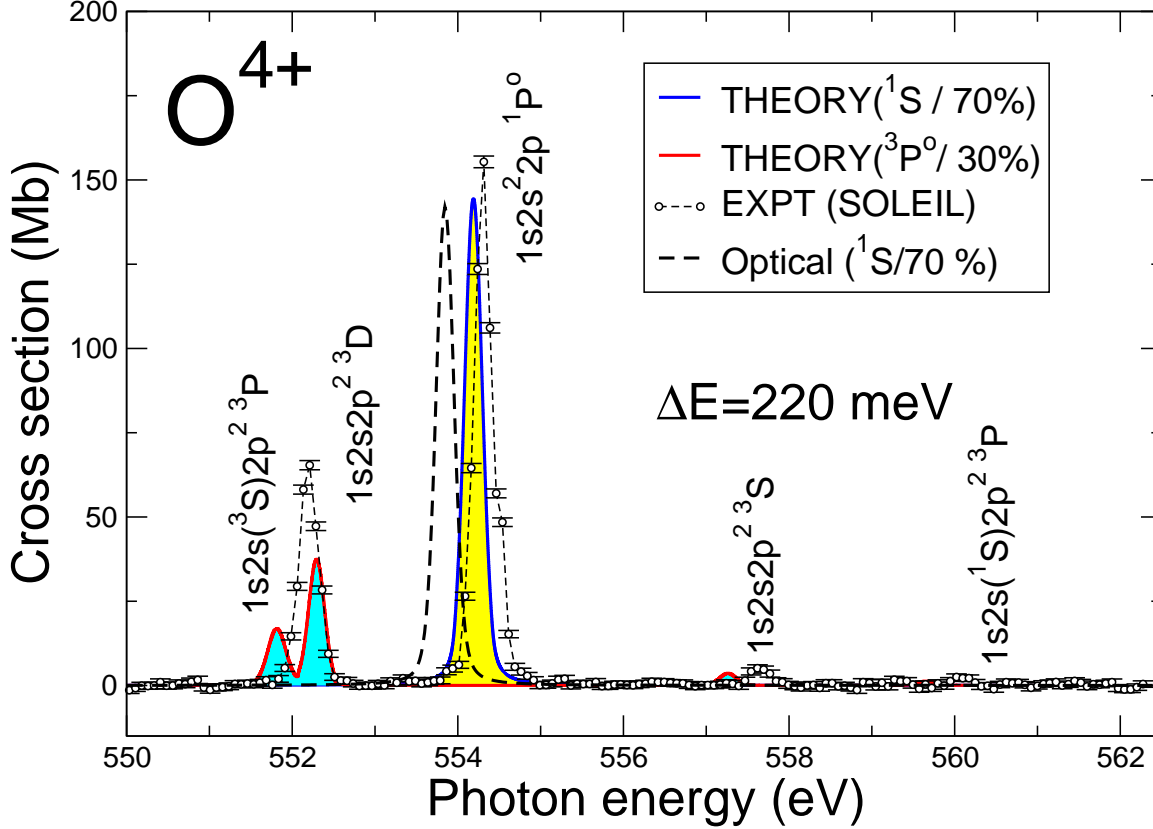


Figure 1. (Colour online) SOLEIL experimental K -shell photoionisation cross section of O^{4+} ions in the 550 - 562 eV photon energy range. Measurements were made with a 220 meV band-pass at FWHM. Solid points are experiment: the error bars represent the statistical uncertainty. Solid lines are the R-matrix plus pseudo-states (RMPS) calculations for the ground (solid blue line) and metastable state (solid red line) with an appropriate admixture, see text for details. Dashed line (black) is the intermediate coupling R-matrix calculations (Garcia et al. 2005), for the ground state only, using the optical potential method. The strong $1s \rightarrow 2p$ resonances are clearly visible in the spectra. The resonance parameters are presented in Table 2 and compared with previous work in the literature.

1999; Burke 2011), using an efficient parallel implementation of the codes (Ballance & Griffin 2006; McLaughlin & Ballance 2015; McLaughlin et al. 2015, 2016, 2017) was used to determine all the cross sections presented here.

Two different basis sets and scattering models were only used in our investigations on the O^{5+} ion. In the first collision model we used Slater orbitals where the $n=3$ physical and $\bar{n}=4$ pseudo-orbitals were used for the residual atomic oxygen ion, O^{6+} , in the K -shell energy region. This basis we designate as basis set A. All the Slater orbitals were generated using the CIV3 structure code (Hibbert 1975).

In the case of O^{5+} ion photoionisation, 17-levels in LS -coupling and 31-levels in intermediate-coupling, were incorporated in our close-coupling approximation for the residual O^{6+} ion, where semi-relativistic effects were included (through the Breit-Pauli approximation). These intermediate coupling Breit-Pauli photoionisation cross-section calcu-

lations were performed in order to gauge the influence of relativistic effects on resonance positions, profiles, and widths for this Li-like system.

In the second approach we used the AUTOSTRUCTURE code (Badnell 1986, 2011) to generate the target wave functions for the subsequent photoionisation cross-section calculations for both of these ions. This we designate as basis set B. For each of the atomic oxygen ions, O^{4+} and O^{5+} , physical orbitals up to $n=3$ were employed. These were augmented with correlation type orbitals $\bar{n}\ell=4\bar{\ell}, \dots, 14\bar{\ell}$, where $\ell=0, 1, 2, 3$, and 4, i.e., s, p, d, f and g, which are Laguerre type pseudo-states. All the computations were performed in LS -coupling. In this approach we used 526-levels in our collision model for the residual O^{5+} ion for photoionisation of O^{4+} . In the case of K -shell O^{5+} photoionisation a collision model was utilised which incorporated 120-levels of the residual O^{6+} ion in the close-coupling approximation.

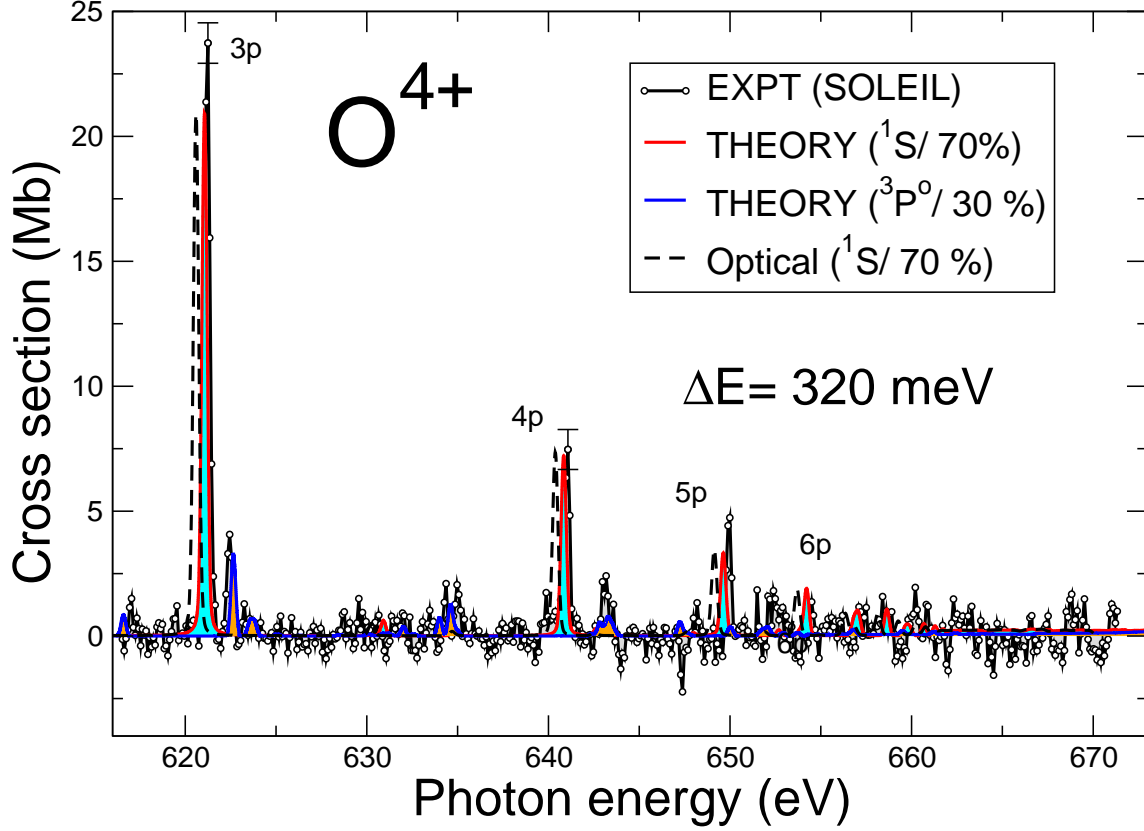


Figure 2. (Colour online) SOLEIL experimental K -shell photoionisation cross section of O^{4+} ions in the 615 - 672 eV photon energy range. Measurements were made with a 320 meV band-pass at FWHM. Open, solid points are experiment: the error bars represent the statistical uncertainty. The solid lines are the R-matrix plus pseudo-states (RMPS) calculations with an appropriate admixture, see text for details. Dashed line (black) is the intermediate coupling R-matrix calculations (Garcia et al. 2005), for the ground state only, using the optical potential method. The strong $1s \rightarrow np$ resonances associated with the $1s^2 2s^2 \ ^1S$ ground state are clearly visible in the spectra. The weaker features in the spectrum are from the $1s^2 2s 2p \ ^3P^o$ metastable state. The resonance parameters are tabulated in Table 3.

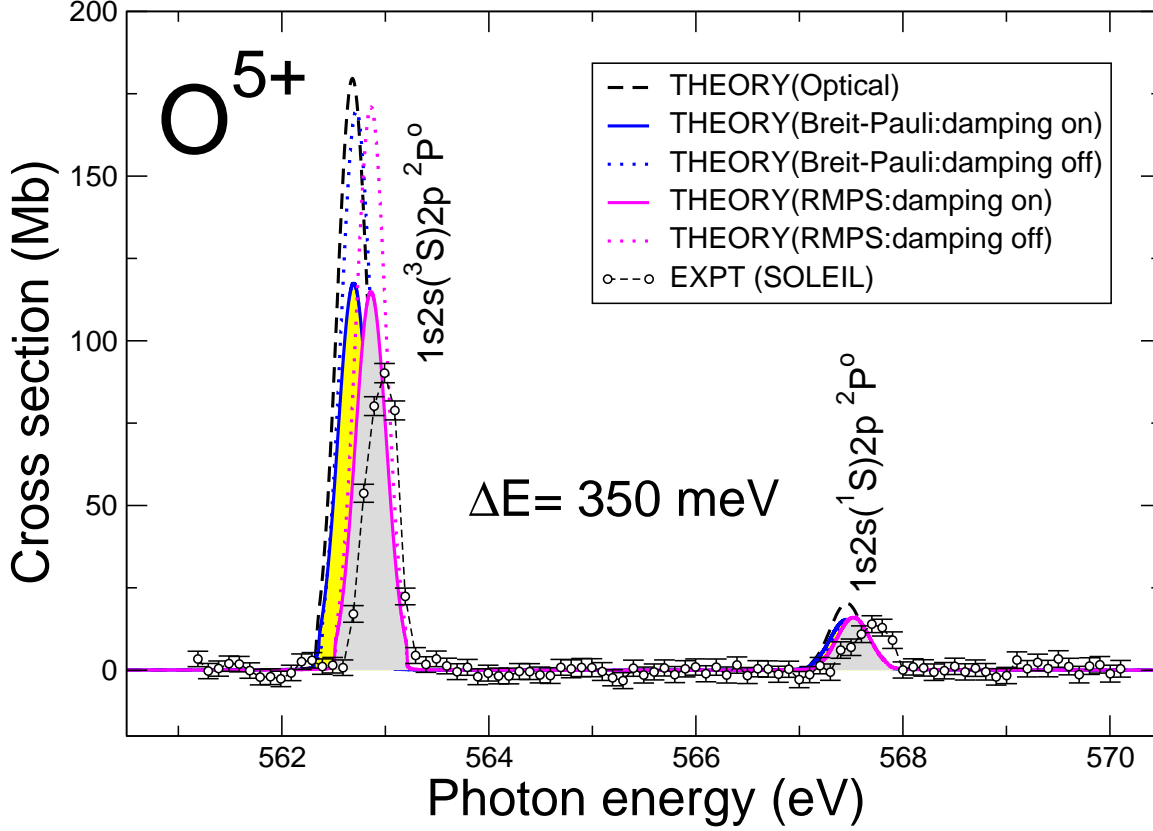


Figure 3. (Colour online) SOLEIL experimental K -shell photoionisation cross section of O^{5+} ions in the 561 - 570 eV photon energy range. Measurements were made with a 350 meV band-pass. Solid points: the error bars give the statistical uncertainty. The dashed (black) line are the intermediate coupling (Breit-Pauli) calculations using the optical potential method (Garcia et al. 2005). The solid (magenta) line are the present RMPS results, and the solid (blue) line are those from the Breit-Pauli approximation, both of which include radiation damping (Robicheaux et al. 1995). The dotted (magenta) line and the dotted (blue) line are the RMPS and Breit-Pauli approximations without radiation damping. The strong $1s \rightarrow 2p$ resonances are clearly visible in the spectra. All the resonance parameters are given in Table 4 and compared with previous work from the literature.

Table 2. Be-like atomic oxygen ions, $1s \rightarrow 2p$ excitation from the $1s^2 2s^2 [^1S] \rightarrow 1s 2s^2 2p [^1P^\circ]$ and $1s^2 2s 2p [^3P^\circ] \rightarrow 1s 2s 2p^2 [^3D, ^3P, ^3S]$ core-excited states. Comparison of experiment, satellite observations and theoretical resonance energies $E_{\text{ph}}^{(\text{res})}$ (eV), natural line widths Γ (meV) and resonance strengths $\bar{\sigma}^{\text{PI}}$ (Mb eV), for the photo-excited $n=2$ states of the O^{4+} ion, in the photon energy region 550 – 562 eV. The SOLEIL experimental determination of the resonances energy gives the uncertainty relative to line 2. For the total uncertainty add 0.15 eV. For the conversion of the satellite wavelength observations to the present energy scale $hc = 1239.841\,974$ eV nm and the absolute error $\Delta E = hc\Delta\lambda/\lambda^2$ in eV were used.

| Resonance (Label) | | SOLEIL (Other Experiments) | SATELLITE (Observation) | R-matrix (Theory) | MCDF (Theory) | OTHERS (Theory) |
|---|--------------------------------|--|--|---|---|--|
| ① $1s^2 2s 2p [^3P^\circ] \rightarrow 1s 2s [^3S] 2p^2 \, ^3P$ | $E_{\text{ph}}^{(\text{res})}$ | – | $550.063^{+0.46m}_{-0.46}$ | 551.816^a | 550.200^d 550.172^d | 551.875^r 552.884^s 551.995^t |
| | Γ | – | | 73^a | 23^d | 13^t |
| | $\bar{\sigma}^{\text{PI}}$ | – | | 4.9^a | | |
| ② $1s^2 2s 2p [^3P^\circ] \rightarrow 1s 2s 2p^2 \, ^3D$ | $E_{\text{ph}}^{(\text{res})}$ | 552.130 ± 0.03^h 552.030 ± 0.80^k | $551.016^{+0.64m}_{-0.64}$ | 552.296^a | 551.100^d 551.175^d | 552.736^r 553.131^s 552.432^t |
| | Γ | 44 ± 6^h | | 42^a | 62^d | 59^t |
| | $\bar{\sigma}^{\text{PI}}$ | 19.8 ± 3^h | | 9.2^a | | |
| ③ $1s^2 2s^2 [^1S] \rightarrow 1s 2s^2 2p \, ^1P^\circ$ | $E_{\text{ph}}^{(\text{res})}$ | 554.250 ± 0.00^h 554.243 ± 0.24^i 554.144 ± 0.07^j 554.370 ± 0.20^l | $554.079^{+0.42m}_{-0.42}$ $553.996^{+0.25n}_{-0.25}$ | 554.189^a 554.550^b $554.739^{c'}$ 553.853^g | 553.150^d 553.241^d 553.117^d | 552.287^e 553.071^f 553.971^r 554.243^s 554.796^t 554.288^u |
| | Γ | 72 ± 4^h | | 66^a 63^c 66^g | 58^d | 72^e 62^f 84^t |
| | $\bar{\sigma}^{\text{PI}}$ | 49 ± 7^h | | 43^a 44^g | | |
| | $E_{\text{ph}}^{(\text{res})}$ | 557.690 ± 0.05^h | $556.757^{+0.53m}_{-0.53}$ $556.330^{+0.10o}_{-0.10}$ $556.050^{+0.70p}_{-0.70}$ $556.732^{+0.50q}_{-0.50}$ | 557.262^a | 556.500^d 556.494^d | 557.508^r 558.563^s 557.798^t |
| | Γ | – | | 40^a | 31^d | |
| | $\bar{\sigma}^{\text{PI}}$ | 2.3 ± 0.3^h | | 0.98^a | | |
| ④ $1s^2 2s 2p [^3P^\circ] \rightarrow 1s 2s [^1S] 2p^2 \, ^3P$ | $E_{\text{ph}}^{(\text{res})}$ | 560.060 ± 0.07^h | | 559.657^a | 560.020^d 560.013^d | 560.203^r 561.243^s |
| | Γ | – | | 74^a | 66^d | |
| | $\bar{\sigma}^{\text{PI}}$ | 0.6 ± 0.1^h | | 0.3^a | | |

^aR-matrix with pseudo-states (RMPS), 526-levels, basis B

^bR-matrix (Berrington et al. 1997) ^cR-matrix (Petrini & Tully 1991), ^{c'}R-matrix (Pradhan et al. 2003)

^dMulti-configuration Dirac Fock (MCDF) (Chen 1985, 1986; Chen & Crasemann 1987b)

^eComplex-scaled multi-reference configuration interaction (CMR-CI) (Zhang & Yeager 2012b)

^fSaddle Point + Complex Rotation (SPCR) (Lin et al. 2001), ^gR-matrix optical potential (Garcia et al. 2005)

^hSOLEIL present work, ⁱEBIT (Gu et al. 2005), ^jEBIT (Schmidt et al. 2004)

^kElectron impact ionisation (Hoffmann et al. 1990), ^lAUGER spectroscopy (Bruch et al. 1987)

^mChandra observations in Mrk 279 (Kaastra et al. 2004)

ⁿChandra observations in NGC 5548, Kaastra 2003 private communication (Schmidt et al. 2004)

^oChandra observations (Liao et al. 2013), ^pChandra observations (Mendoza et al. 2012)

^qXMM - Newton observations (Blustin et al. 2002)

^rCowan code (Kaastra et al. 2004), ^sHULLAC code (Kaastra et al. 2004)

^tSCUNC present work see text for details, ^uFAC code Gu (2010) private communication (Liao et al. 2013).

Table 3. Be-like atomic oxygen ions, $1s \rightarrow np$ excitation from the $1s^2 2s^2 [^1S] \rightarrow 1s 2s^2 np [^1P^\circ]$ and $1s^2 2s 2p [^3P^\circ] \rightarrow 1s 2s 2p np [^3D, ^3P, ^3S]$ ($n > 2$) core-excited states. Comparison of experiment, satellite observations and theoretical resonance energies $E_{\text{ph}}^{(\text{res})}$ (eV), natural line widths Γ (meV) and resonance strengths $\bar{\sigma}^{\text{PI}}$ (Mb eV), for the photo-excited states of the O^{4+} ion, in the photon energy region 615 – 675 eV. The SOLEIL experimental determination of the resonances energy gives the uncertainty relative to line 2. For the total uncertainty add 0.15 eV. For the conversion of the satellite wavelength observations to the present energy scale $hc = 1239.841\,974$ eV nm and the absolute error $\Delta E = hc\Delta\lambda/\lambda^2$ in eV were used.

| Resonance (Label) | | SOLEIL (Other Experiments) | SATELLITE (Observation) | R-matrix (Theory) | MCDF (Theory) | OTHERS (Theory) |
|--|--------------------------------|-------------------------------|---------------------------------|----------------------------|------------------|--------------------|
| $1s^2 2s^2 [^1S] \rightarrow 1s 2s^2 3p \, ^1P^\circ$ (5) | $E_{\text{ph}}^{(\text{res})}$ | 621.230 ± 0.05^e | – | 621.063^a 620.604^b | – | 622.137^f |
| | Γ | – | | 80^a 54^b | | 94^f |
| | $\bar{\sigma}^{\text{PI}}$ | 8.6 ± 1.3^e | | 8.4^a 8.3^b | | |
| Resonance (6) | $E_{\text{ph}}^{(\text{res})}$ | 622.440 ± 0.07^e | – | 622.653^a | – | |
| | Γ | – | | 11^a | | |
| | $\bar{\sigma}^{\text{PI}}$ | 1.4 ± 0.2^e | | 1.1^a | | |
| $1s^2 2s^2 [^1S] \rightarrow 1s 2s^2 4p \, ^1P^\circ$ (7) | $E_{\text{ph}}^{(\text{res})}$ | 641.040 ± 0.06^e | $641.408 \, ^{+0.55}_{-0.55}^d$ | 640.841^a 640.388^b | – | 641.852^f |
| | Γ | – | | 78^a 52^b | | 67^f |
| | $\bar{\sigma}^{\text{PI}}$ | 3.6 ± 0.5^e | | 2.9^a 3^b | | |
| Resonance (8) | $E_{\text{ph}}^{(\text{res})}$ | 643.120 ± 0.09^e | – | 643.273^a | – | – |
| | Γ | – | | 7^a | | |
| | $\bar{\sigma}^{\text{PI}}$ | 1.2 ± 0.2^e | | 0.2^a | | |
| $1s^2 2s^2 [^1S] \rightarrow 1s 2s^2 5p \, ^1P^\circ$ (9) | $E_{\text{ph}}^{(\text{res})}$ | 649.940 ± 0.07^e | $650.494 \, ^{+0.56}_{-0.56}^d$ | 649.630^a 649.143^b | – | 650.978^f |
| | Γ | – | | 78^a 55^b | | 48^f |
| | $\bar{\sigma}^{\text{PI}}$ | 2.7 ± 0.4^d | | 1.4^a 1.4^b | | |

^aR-matrix with pseudo-states (RMPS), 526-levels, basis B

^bR-matrix optical potential (Garcia et al. 2005)

^cMulti-configuration Dirac Fock (MCDF) (Chen 1985, 1986; Chen & Crasemann 1987b)

^dXMM - Newton observations in NGC 3783 (Behar et al. 2003)

^eSOLEIL present work

^fSCUNC present work, see text for details

Table 4. Li-like atomic oxygen ions, $1s \rightarrow 2p$ excitation from the $1s^2 2s[^2S] \rightarrow 1s(2s2p\ ^1P^\circ)[^2P^\circ]$ and $1s(2s2p\ ^3P^\circ)[^2P^\circ]$ core-excited states. Comparison of experiment, satellite observations and theoretical results for the resonance energies $E_{\text{ph}}^{(\text{res})}$ (eV), natural line widths Γ (meV) and resonance strengths $\bar{\sigma}^{\text{PI}}$ (Mb eV), for the photo-excited $n=2$ states of the O^{5+} ion, in the photon energy region 560 – 570 eV with previous investigations. The uncertainty of the SOLEIL experiment energy of the lines is relative to line A. For the total uncertainty, add 0.15 eV for energy calibration. For the conversion of the satellite wavelength observations to the present energy scale $hc = 1239.841\,974$ eV nm and the absolute error $\Delta E = hc\Delta\lambda/\lambda^2$ in eV were used.

| Resonance (Label) | | SOLEIL (Other Experiments) | SATELLITE (Observation) | R-matrix (Theory) | MCDF (Theory) | OTHERS (Theory) |
|--|--------------------------------|-------------------------------|--------------------------------|---|------------------|---|
| $1s^2 2s[^2S] \rightarrow 1s(2s2p\ ^3P^\circ)[^2P^\circ]$ (A) | $E_{\text{ph}}^{(\text{res})}$ | 562.940 ± 0.00^j | $562.662^{+0.70^q}_{-0.70}$ | 562.860^a | 562.018^d | 562.829^e |
| | | 563.000 ± 1.00^k | $562.899^{+0.10^r}_{-0.10}$ | $562.709^{a'}$ | 563.039^d | 562.415^f |
| | | 563.119 ± 0.20^n | $562.950^{+0.08^s}_{-0.08}$ | 562.297^b | 562.803^d | 563.440^g |
| | | 563.068 ± 0.04^o | $562.828^{+0.06^t}_{-0.06}$ | 562.680^c | | 563.057^h |
| | | 563.053 ± 0.15^p | $563.309^{+0.05^u}_{-0.26}$ | | | 562.534^x |
| | | 563.100 ± 0.20^m | $562.287^{+0.40^v}_{-0.40}$ | | | $562.705^{i'}$ |
| | | | $562.465^{+0.10^y}_{-0.10}$ | | | |
| | | | $562.912^{+0.24^z}_{-0.23}$ | | | |
| | | | $563.053^{+0.51^{z'}}_{-0.51}$ | | | |
| | Γ | – | | 6^a $6^{a'}$ 4^b 9^c | 5^d | 6^e 4^f 6^g $6^{i'}$ |
| | $\bar{\sigma}^{\text{PI}}$ | 36 ± 5^j | | 42.52^a $42.52^{a'}$ 71.3^c | | |
| $1s^2 2s[^2S] \rightarrow 1s(2s2p\ ^1P^\circ)[^2P^\circ]$ (B) | $E_{\text{ph}}^{(\text{res})}$ | 567.620 ± 0.05^j | $566.915^{+0.40^v}_{-0.40}$ | 567.519^a | 568.499^d | 567.420^e |
| | | 566.081 ± 0.12^l | | $567.445^{a'}$ | | 567.420^f |
| | | 567.719 ± 2.00^m | | 566.987^b | | 568.117^g |
| | | 568.000 ± 2.00^n | | 567.450^c | | 567.783^i |
| | | 567.563 ± 0.26^p | | | | $567.762^{i'}$ |
| | Γ | – | | 46^a $46^{a'}$ 45^b 48^c | 49^d | 46^f 50^g 45^i $59^{i'}$ |
| | $\bar{\sigma}^{\text{PI}}$ | 7.4 ± 1^j | | 6.4^a $6.3^{a'}$ 8.6^c | | |

^aR-matrix with pseudo-states (RMPS), 120-levels, basis B, ^{a'}R-matrix, Breit-Pauli, 31-levels, basis A

^bR-matrix (Pradhan et al. 2003)

^cR-matrix, optical potential method, intermediate coupling (Garcia et al. 2005)

^dMulti-configuration Dirac Fock (MCDF) (Chen 1985, 1986; Chen & Crasemann 1987a)

^eComplex-scaled multi-reference configuration interaction (CMR-CI) (Zhang & Yeager 2012a)

^fSaddle Point + Complex Rotation (SPCR) (Bingcong & Wensheng 2000)

^gSaddle Point + Complex Rotation (SPCR) (Wu & Xi 1991)

^hIntermediate-coupling (Gabriel 1972)

ⁱSaddle Point Method (SPM) (Davis & Chung 1989), ^{i'}SCUNC present work, see text for details

^jSOLEIL present work, ^kAuger Spectroscopy (Bruch et al. 1979), ^lEBIT (Gu et al. 2005)

^mAuger Spectroscopy (Bruch et al. 1987), ⁿElectron-impact ionisation experiments (Hoffmann et al. 1990)

^oEBIT (Schmidt et al. 2004), ^pLaser plasma experiment (Nicolosi & Tondello 1997)

^qChandra observations (Mendoza et al. 2012)

^rChandra observations (Yao et al. 2009), ^sChandra observations (Gatuzz et al. 2013a,b)

^tChandra observations (Liao et al. 2013)

^uChandra observations in NGC 5548, Kaastra (2003) private communication (Schmidt et al. 2004)

^vChandra observations in NGC 5548 (Kaastra et al. 2002), ^xFAC code Gu (2010) private communication (Liao et al. 2013)

^yChandra observations in MCG-6-30-15 (Lee et al. 2001)

^zXMM-Newton observations in Cyg X-2 (Cabot et al. 2013)

^{z'}XMM-Newton observations in Mkn 501 RGS1 (Nicastrro et al. 2016b)

MNRAS **000**, 1–17 (2016)

3.3 Be-like atomic oxygen ions

For the O^{4+} ion we used the R-matrix with pseudo-states method to perform all the photoionisation cross sections. All the photoionisation cross section calculations were performed in LS -coupling. We note that the ion-beam in the SOLEIL experiments contain both ground state and metastable states. Photoionisation cross-section calculations were carried out for both these initial states of O^{4+} ; $1s^2 2s^2 {}^1S$ ground state and the $1s^2 2s 2p {}^3P^o$ metastable state. Thirty-five continuum orbitals were utilised in the collision calculations. In our collision model we retained 526-levels in the close-coupling expansion and basis set B was utilised for this scattering approximation. A boundary radius of 13.838 Bohr was required to cater for the very diffuse pseudo-states. In the outer region we used an energy mesh of $1.36 \mu\text{eV}$ to fully resolve all the fine resonance features in the cross sections.

3.4 Li-like atomic oxygen ions

For the O^{5+} ion we used the R-matrix with pseudo-states method (RMPS) and the Breit-Pauli approximation to perform all the photoionisation cross sections. Basis set A was used with 17 levels included in LS -coupling and 31 levels in the intermediate-coupling approximation for the residual O^{6+} ion. In the SOLEIL measurements, for this ion, only the ground-state is present, so cross section calculations were performed for the $1s^2 2s^2 {}^1S$ ground state of O^{5+} in LS and in intermediate coupling taking into account relativistic effects through the Breit-Pauli (BP) approximation.

Thirty-five continuum orbitals were utilised in the collision calculations and a boundary radius of 6.0 Bohr to accommodate the diffuse $n=4$ orbitals for basis A. For the R-matrix with pseudo-states approach, 120-levels were retained in the close-coupling approximation, with basis set B. A boundary radius of 11.925 Bohr was required to cater for the very diffuse pseudo-states and thirty-five continuum orbitals used for the collision calculations.

Photoionization cross-section calculations for O^{5+} ions were performed both in LS and intermediate coupling. The intermediate coupling calculations were carried out using the semi-relativistic Breit-Pauli approximation which allows for relativistic effects to be included. Radiation-damping (Robicheaux et al. 1995) effects were also included within the confines of the R-matrix approach (Burke 2011) for completeness as this affects only narrow resonances found in cross-sections for highly charged systems. For the O^{5+} ion an energy mesh of $680 \mu\text{eV}$ resolved all the resonance features in the spectra for the photon energy range 560 - 575 eV.

4 RESULTS AND DISCUSSION

Fig 1 illustrates the experimental and theoretical results for the O^{4+} ion in the photon energy region 550 - 562 eV where the strong $1s \rightarrow 2p$ resonances are found. The theoretical cross sections were convoluted with an appropriate Gaussian profile having a similar band width to the SOLEIL measurements; 220 meV for the region 550 - 565 eV. An admixture of the ground and metastable states was applied to simulate experiment. We found that 70% of the $1s^2 2s^2 {}^1S$ ground and

30 % of the $1s^2 2s 2p {}^3P^o$ metastable states suitably matched theory with experiment. In Fig. 2 we present the photon energy region 615 - 670 eV where the $1s \rightarrow np$ resonance features are located. Here again a similar admixture (70% ground state and 30% metastable state) for the theoretical cross sections, after convolution by a Gaussian profile with 320 meV FWHM, simulates the experimental results very well. Tables 2 and 3 compare our experimental and theoretical results for the resonance parameters for this Be-like systems with other theoretical, experimental and satellite observations. Figs 1 and 2 includes the intermediate-coupling calculations of Garcia and co-workers (Garcia et al. 2005) performed using the optical potential method (dashed black line) convolved by the Gaussian profiles and weighted by 70% for the ground state only for completeness.

The results for the resonance strengths σ^{PI} found in the O^{4+} spectra are presented in Tables 2 and 3 and the resonance strengths have been weighted by the 70% and 30% admixture for the ground and metastable states to compare directly with experiment.

For the O^{4+} ion it should be noted that from a comparison of the experimental and R-matrix resonance strengths σ^{PI} (see Fig. 1 and Fig. 2) excellent agreement, particularly for the strong resonant features (due to the $1s^2 2s^2 {}^1S$ ground state) in the spectrum is achieved. It can be seen from Tables 2 and 3, the agreement between experiment and theory for the weaker resonant features in the spectra of O^{4+} (due to the $1s^2 2s 2p {}^3P^o$ metastable) is not as good compared to the ground state. The weak resonances 6 and 8 in Table 3 (originating from the $1s^2 2s 2p {}^3P^o$ metastable state) may be identified with the aid of quantum defect theory. The weak resonance profiles of the remaining members of the Rydberg series emanating from the $1s^2 2s 2p {}^3P^o$ metastable state make them difficult to resolve experimentally.

Fig. 3 shows a comparison of the SOLEIL cross-section measurements made with a band-pass of 350 meV FWHM for the O^{5+} ion with our theoretical results which include and exclude radiation damping (Robicheaux et al. 1995). In order to compare directly with experiment, theory has been convoluted with a Gaussian profile having a similar width of 350 meV at FWHM. The results from both the Breit-Pauli (BP) approximation (using basis A) and those from the R-matrix with pseudo-states method (using basis B) are shown. As seen from Fig. 3 the calculations of Garcia and co-workers (Garcia et al. 2005) performed (using the optical potential approach) in intermediate-coupling, would appear to not include radiation damping (Robicheaux et al. 1995), as they are similar to our Breit-Pauli results without radiation damping, and as such overestimate the resonance strength of the narrow resonance located by experiment at 562.94 eV. As illustrated in Fig. 3 and from the results presented in Table 4, the R-matrix with pseudo-states (RMPS) cross sections (that include radiation damping) give best agreement with the present measurements from the SOLEIL radiation facility for this ion in the photon energy region where the resonances of O^{5+} are located.

An additional check on the theoretical data is the comparison of the integrated oscillator strength f or the resonance strength with experiment. The quantity f for the theoretical and experimental spectra may be determined for each resonance using (Shore 1967; Fano & Cooper 1968;

Table 5. Li-like and Be-like ions, integrated oscillator strength for the core-excited states arising from respectively the ground configurations $1s^2 2s$ and $1s^2 2s^2$ of each ion. The table shows a comparison of the present experimental and theoretical results for the integrated oscillator strengths f for the dominant core photo-excited $n=2$ states of the first four ions of each sequences (Z , is the atomic number of the ion) along with previous investigations.

| Z | ION | | EXPERIMENT | THEORY |
|---------|---|-----|--------------------|--------------|
| Li-like | $1s^2 2s \rightarrow 1s[2s2p \ ^3P] \ ^2P^o$ | | Resonance | |
| 5 | B^{2+} | f | 0.465 ± 0.09^a | $0.413^{a'}$ |
| 6 | C^{3+} | f | 0.483 ± 0.10^b | $0.485^{b'}$ |
| 7 | N^{4+} | f | 0.413 ± 0.07^c | 0.546^i |
| 8 | O^{5+} | f | 0.328 ± 0.05^d | 0.387^j |
| Be-like | $1s^2 2s^2 \ ^1S \rightarrow 1s2s^2 2p \ ^1P^o$ | | Resonance | |
| 5 | B^+ | f | 0.641 ± 0.13^e | 0.413^g |
| 6 | C^{2+} | f | 0.624 ± 0.10^f | 0.447^h |
| 7 | N^{3+} | f | 0.650 ± 0.10^c | 0.546^i |
| 8 | O^{4+} | f | 0.640 ± 0.09^d | 0.559^j |

^aALS, experiment (Müller et al. 2010), ^bALS, experiment (Müller et al. 2009)

^{a'}R-matrix, theory (Müller et al. 2010), ^{b'}R-matrix, theory (Müller et al. 2009)

^cSOLEIL, experiment (Al Shorman et al. 2013), ^dSOLEIL, experiment present work.

^eALS, experiment (Müller et al. 2014), ^fALS, experiment (Scully et al. 2005)

^gR-matrix,theory (Müller et al. 2014), ^hR-matrix,theory (Scully et al. 2005)

ⁱR-matrix,theory (Al Shorman et al. 2013), ^jR-matrix,theory present work

Berkowitz 1979),

$$f = 9.1075 \times 10^{-3} \sigma^{\text{PI}}. \quad (5)$$

The resonance strength in the photoionisation cross-section σ^{PI} is defined as

$$\sigma^{\text{PI}} = \int_{E_1}^{E_2} \sigma(h\nu) dh\nu, \quad (6)$$

where $[E_1, E_2]$ is the photon energy range over which each resonance profile extends.

Fig. 4 illustrates results for the oscillator strengths f along the Li-like and Be-like iso-electronic sequences, for the strong K_α transitions originating from the ground state of each ion. Table 5 tabulates these integrated oscillator strengths f results obtained from synchrotron radiation (SR) measurements (ALS and SOLEIL) and from R-matrix calculations. For the Be-like sequence the values have been corrected for ground state populations. As can be seen from Table 5 and Fig. 4, apart from Be-like boron and to a lesser extent Be-like carbon, the agreement between theory and experiment along both iso-electronic sequences is quite satisfactory giving further confidence in our current work.

5 COMPARISON WITH SATELLITE OBSERVATIONS

In Tables 2, 3, and 4 comparisons are made with the available experimental and satellite observations in the literature

for resonance energies for Be-like and Li-like atomic oxygen ions. One can clearly see various discrepancies between our present ground based measurements, made at SOLEIL, and the Chandra and XMM-Newton satellite observations. We note that for both atomic ions, the R-matrix with pseudostates results favour those from the SOLEIL radiation facility.

Fig 5 illustrates a comparison of various ground based synchrotron cross section measurements (ALS and SOLEIL) for the atomic oxygen isonuclear sequence in the wavelength region 21 – 24 Å with the low-energy-transmission-grating (LETG) spectra observed by Chandra for the blazar Mkn 421 ACIS (Nicastro et al. 2016a). One clearly sees, especially for low charged stages of oxygen ions, discrepancies in the resonance energies for the strong K_α lines in the Chandra spectra compared to the different ground based light source measurements which we discuss and quantify. The satellites observe OI to OIV lines (with a shift) and noshift in the OV and OVI lines, as seen in the comparison with the spectra for the blazar Mkn 421 (Nicastro et al. 2016a), shown in Fig 5. Similar effects are also seen in the spectra of H 2356-309 LETG, H 2356-309 RGS1, and Mkn 501 RGS1, for the wavelength region 21 – 24 Å in the recent observations of Nicastro and co-workers (Nicastro et al. 2016a,b). We note similar differences are seen in the wavelength region 21 – 24 Å, for satellite observations in the high-energy-transmission grating (HETG) spectra observed by Chandra for the x-ray

Table 6. Comparison of the energies for the K_α resonance line (centroid in eV), ions in their ground state, along the atomic oxygen isonuclear sequence. The entries in the table are from synchrotron radiation light source (SR) and EBIT measurements, compared to available Chandra and XMM-Newton satellite observations. For conversion of the satellite wavelength observations to the present energy scale $hc = 1239.841\,974$ eV nm was used.

| Atomic Oxygen | SR | EBIT | | <i>Chandra and XMM</i> | |
|---------------|-------------------------|-------------------------|-----------------------|--------------------------|-----------------------|
| Ionised state | E (eV) | E(eV) | $\Delta E(\text{eV})$ | E(eV) | $\Delta E(\text{eV})$ |
| OI | 526.79(4) ^a | | | 527.39(2) ^g | -0.60 |
| | | | | 527.37(40) ^o | -0.58 |
| | | | | 527.44(18) ^p | -0.65 |
| OII | 530.50(13) ^b | | | 530.97(3) ^g | -0.47 |
| | | | | 530.98(40) ^o | -0.48 |
| OIII | 536.86(13) ^b | 537.42(9) ^e | -0.55 | 537.94(2) ^g | -1.08 |
| OIV | 544.52(13) ^c | 545.20(10) ^e | -0.68 | 546.22(8) ^g | -1.74 |
| | | | | 546.43(24) ^p | -1.91 |
| OV | 554.25(18) ^d | 554.14(7) ^f | 0.11 | 556.33(9) ^{g,*} | -2.08 |
| | | | | 554.00(25) ^h | -0.25 |
| | | | | 554.08(42) ⁱ | 0.17 |
| OVI | 562.94(18) ^d | 563.07(4) ^d | -0.13 | 562.83(6) ^g | 0.11 |
| | | | | 562.90(10) ^j | 0.04 |
| | | | | 562.95(10) ^k | -0.01 |
| | | | | 563.31(26) ^h | -0.63 |
| | | | | 562.29(40) ^l | 0.65 |
| | | | | 562.47(10) ^m | 0.47 |
| | | | | 562.90(25) ⁿ | 0.04 |
| | | | | 563.05(51) ^p | -0.11 |

^a Advanced Light Source (McLaughlin et al. 2013a,b)

^b SOLEIL (Bizau et al. 2015)

^c SOLEIL (McLaughlin et al. 2014; Bizau et al. 2015)

^d SOLEIL present results

^e EBIT (Gu et al. 2005)

^f EBIT (Schmidt et al. 2004)

^g Chandra (Liao et al. 2013)

^h Chandra Kaastra 2003, private communication, (Schmidt et al. 2004)

ⁱ Chandra (Kaastra et al. 2004)

^j Chandra (Yao et al. 2009)

^k Chandra (Gatuzz et al. 2013a,b)

^l Chandra (Kaastra et al. 2002)

^m Chandra (Lee et al. 2001)

ⁿ XMM - Newton (Cabot et al. 2013)

^o Chandra and XMM-Newton (Nicastro et al. 2016a)

^p Chandra and XMM-Newton (Nicastro et al. 2016b)

*OV line observed by Liao et al. (2013), is the OII K_β line (at 556.48(50) eV), confirmed recently by Nicastro et al. (2016a).

binary XTE J1817-332 (Gatuzz et al. 2013a,b), although no OIV or OV K-lines are observed.

Fig 6 illustrates more precisely the discrepancies for the O^{4+} and O^{5+} ions, K_α resonance lines between ground based experiments and prior satellite observations. The present results are for the O^{4+} (OV) ion (top panel) and the O^{5+} (OVI) ion (bottom panel). Table 6 quantifies the differences between the ground based experimental measurements (Synchrotron radiation (SR), and EBIT), and the satellite observations (Chandra, and XMM-Newton). We note in passing that the measurements performed at two independent ground based light source experiments highlighted discrepancies in the energies of the K_α lines along the atomic oxy-

gen iso-nuclear sequence compared to satellite observations. Furthermore, we point out that the Chandra observations of Liao and co-workers (Liao et al. 2013), particularly for the OV line at 556.33 eV appears to be a misidentification. This line is instead identified as the OII K_β line. We have indicated this in Fig. 6. This mis-identification was indicated in the observations of Gatuzz and co-workers (Gatuzz et al. 2014) and confirmed by the definitive observations of Nicastro and co-workers (Nicastro et al. 2016a), who found the OII K_β line at 556.482 ± 0.50 eV from the average of 29 x-ray sources.

The discrepancies with the satellite observations are as yet not fully understood (Kallman 2016). We note, for the

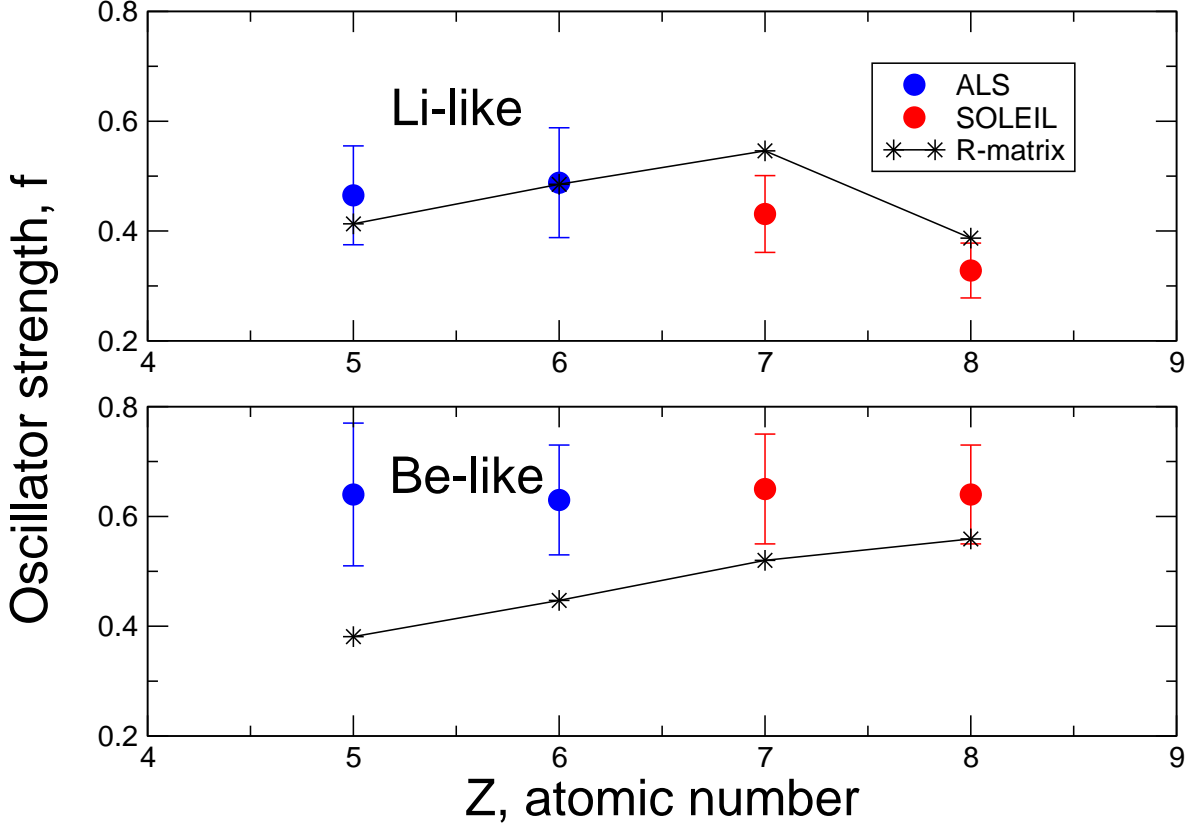


Figure 4. (Colour online) Comparison of the integrated oscillator strengths f obtained from synchrotron radiations measurements with R-matrix calculations. The solid circle are from the ALS (blue) and SOLEIL (red) radiation facilities, respectively, for the Li-like and Be-like iso-electronic sequences. The asterisk values (black) are from R-matrix calculations.

Table 7. Comparison of the calibrated energies from the EELS and PES experimental methods (Bizau et al. 2015). The energy difference between the two experimental methods is at most 0.22 eV.

| O ₂ K-shell | EELS | PES | ΔE (eV) |
|--------------------------|-------------------------|------------|-----------------|
| 1s $\rightarrow \pi^*$ | 530.80(20) ^a | 530.70(15) | -0.10 |
| 1s $\rightarrow 3\sigma$ | 538.95(4) ^b | 539.17(15) | +0.22 |

^aHitchcock & Brion (1980)

^bTanaka et al. (2008)

synchrotron measurements, the energy calibration was originally based on Electron Energy Loss Spectroscopy (EELS) measurements of O₂ 1s $\rightarrow \pi^*$ performed by Hitchcock & Brion (1980) and ion yield measurements of O₂ 1s $\rightarrow 3\sigma$ by Tanaka et al. (2008). More recently the energy calibration is based on O₂ K-shell absorption spectra and Photo Electron

Spectroscopy (PES) for 2s removal in Neon (Bizau et al. 2015). As can clearly be seen from Table 7 the difference between the two types of energy calibrations is the order of 0.22 eV, and therefore cannot account for the larger energy differences with the satellite observations. Further independent ground based synchrotron light sources measurements would be of great beneficial help to try and minimise this source of calibration error.

6 CONCLUSIONS

For the first time high-resolution photoionisation cross-section measurements have been made on Be-like and Li-like atomic oxygen ions in the vicinity of their strong 1s \rightarrow 2p resonances and in the 1s \rightarrow np resonant region for O⁴⁺ ions. The measurements are compared with theoretical results from the R-matrix approach, the SCUNC method, and with available satellite observations. Resonance features present in the spectra and predicted by the R-matrix with pseudo-

Chandra LETG Spectra: Mkn421-ACIS

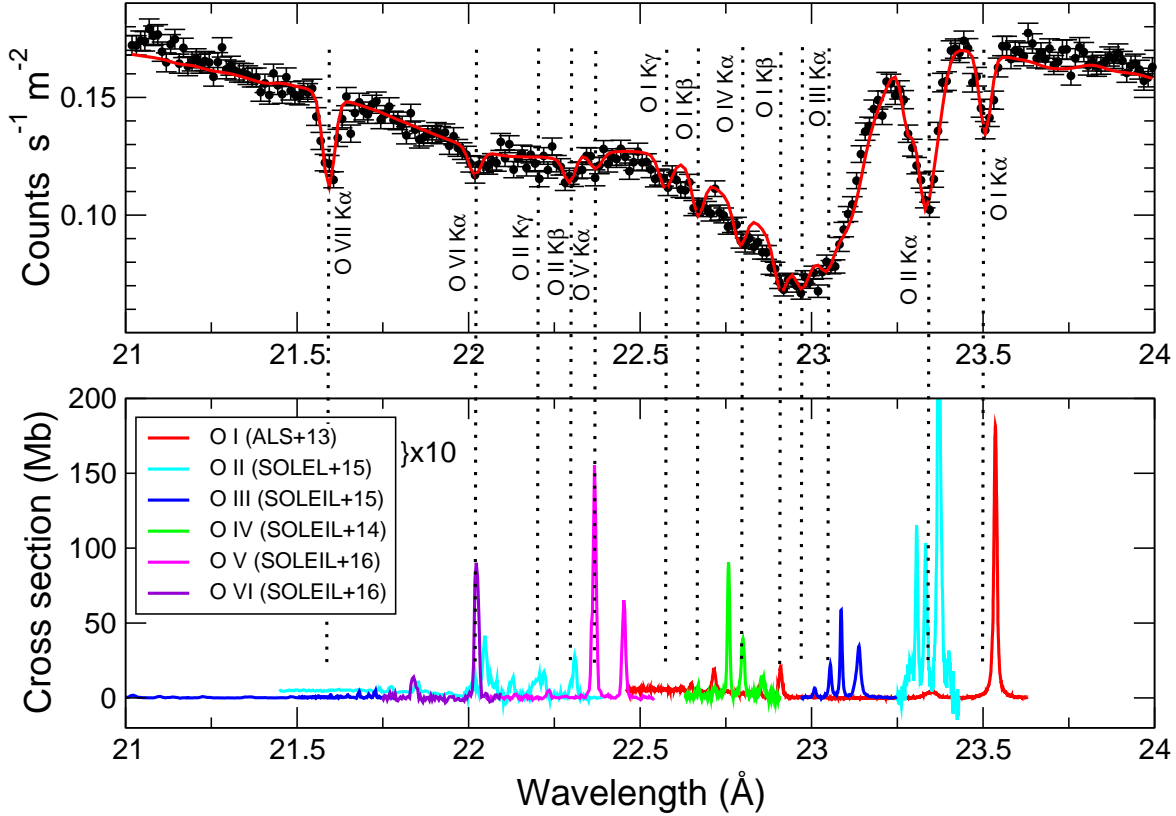


Figure 5. (Colour online) Top panel, Chandra LETG spectra for the blazar Mkn 421 ACIS in the wavelength 21 - 24 Å composed from several different exposures with the Chandra satellite (Nicastro et al. 2016a). Bottom panel, for the same wavelength range, measurements are illustrated from a combination of ground based experimental spectra made at various synchrotron radiation facilities; Advanced Light Source (O I) (McLaughlin et al. 2013a,b), SOLEIL (O II and O III) (Bizau et al. 2015) SOLEIL (O IV) (McLaughlin et al. 2014) and the present SOLEIL (OV and O VI) results. The strongest lines in the synchrotron measurements are from the ground state of each ionised stage of atomic oxygen. The weaker ones in the measurements are from the metastable states of each ionic complex. The OI and OII results are scaled by a factor of 10.

states (RMPS) method show excellent agreement with the measurements made at the SOLEIL radiation facility. A detailed comparison of our results (for both systems) are in agreement with predictions from other similar highly sophisticated theoretical approaches. Within the R-matrix approach, we note that both basis sets and models gave suitable results compared to experiment. The collision models with basis set B gave the more favourable results compared to experiment.

A detailed analysis of the resonance parameters indicates some differences with the present SOLEIL experimental results, particularly for the weaker resonance strengths in the O^{4+} spectrum. We speculate that this may be due to the lack of electron correlation included in our theoretical model. We have highlighted various discrepancies with previous satellite observations. Overall the theoretical resonance

positions are in suitable agreement with current ground based SOLEIL experimental measurements. The theoretical cross-section data has been benchmarked against high resolution measurements and as such would be suitable to be incorporated into databases such as CLOUDY (Ferland et al. 1998; Ferland 2003), XSTAR (Kallman & Bautista 2001) and AtomDB (Foster et al. 2012) that are widely used for astrophysical modelling.

ACKNOWLEDGMENTS

The authors would like to thank the SOLEIL staff, in particular, J. Bozek and S. Nandi for their helpful assistance during the measurements. We thank F. Nicastro for the provision of the Chandra spectra for the blazar Mkn 421 and illuminating discussions on the differences with the Chandra

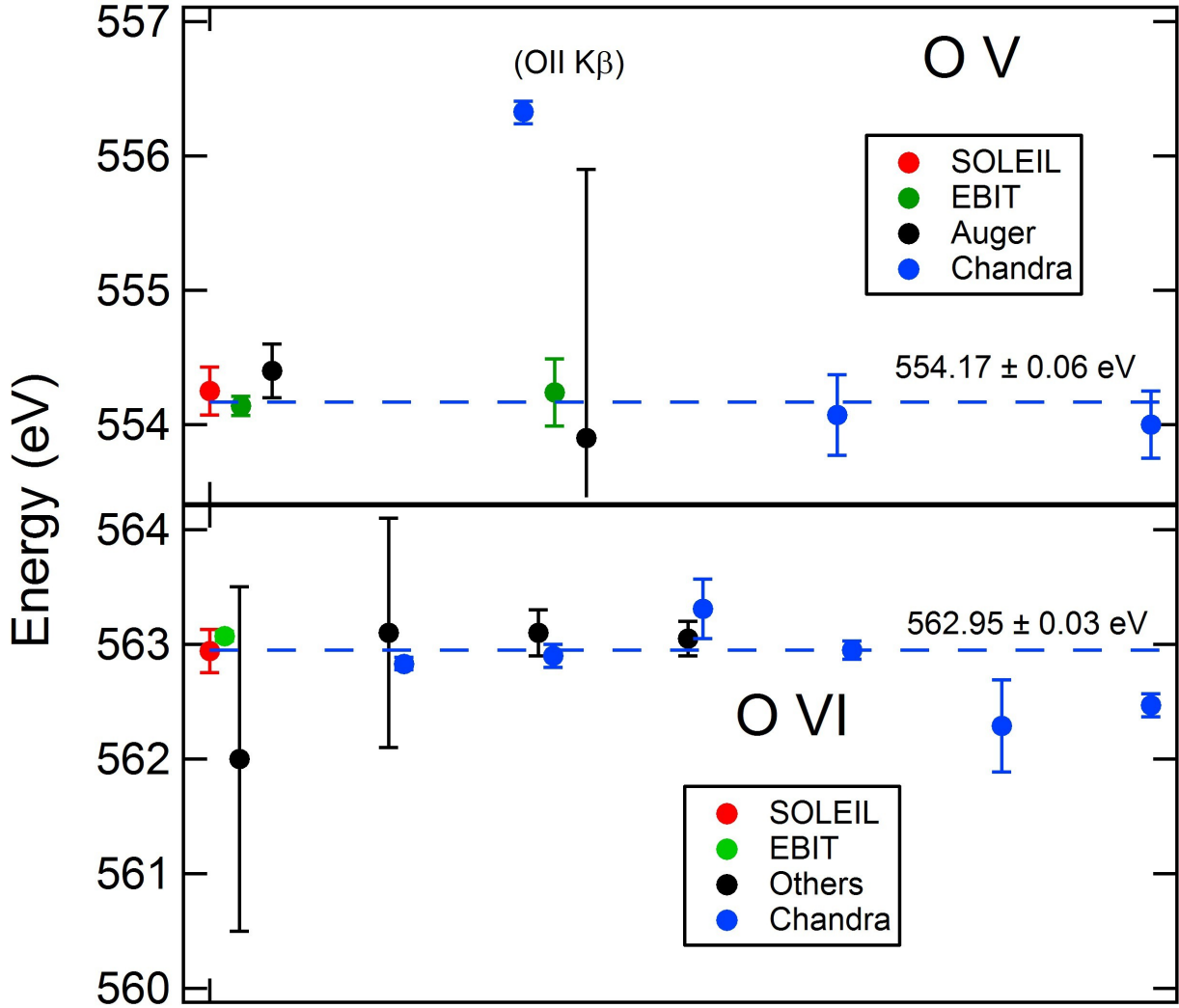


Figure 6. (Colour online) Top panel, comparison of the K_α energies for O^{4+} ions with values obtained from various experimental approaches, EBIT, Auger, the current SOLEIL measurements and Chandra observations. Bottom panel, similarly for the K_α energies for O^{5+} ions with various experimental and observations with the current SOLEIL measurements. The dashed line (blue) in both panels is the ponderated mean of all the values.

observations. T. R. Kallman, at Nasa Goddard, J. C. Raymond and R. K. Smith at the Harvard-Smithsonian Center for Astrophysics are also thanked for discussions on the astrophysical applications. B. M. M. acknowledges support from the U.S. National Science Foundation through a grant to ITAMP at the Harvard-Smithsonian Center for Astrophysics, the RTRA network Triangle de la Physique and Queen's University Belfast for the award of a Visiting Research Fellowship (VRF). MFG acknowledges Qatar University for funding support through the startup grant No. QUSG-CAS-DMSP-14/15-4. The R -matrix computational work was performed at the National Energy Research Scientific Computing Center (NERSC) in Berkeley, CA, USA

and at the High Performance Computing Center Stuttgart (HLRS) of the University of Stuttgart, Stuttgart, Germany. Grants of computational time at the National Energy Research Scientific Computing Center in Berkeley, CA, USA and at the High Performance Computing Center Stuttgart (HLRS) of the University of Stuttgart, Stuttgart, Germany are gratefully acknowledged.

REFERENCES

Al Shorman M. M., et al., 2013, *J. Phys. B: At. Mol. Opt. Phys.*, **46**, 195701

- Badnell N. R., 1986, *J. Phys. B: At. Mol. Opt. Phys.*, **19**, 382
- Badnell N. R., 2011, *Comput. Phys. Commun.*, **182**, 1528
- Ballance C. P., Griffin D. C., 2006, *J. Phys. B: At. Mol. Opt. Phys.*, **39**, 3617
- Behar E., Rasmuseen A. P., Blustin A. J., Sako M., Kahn S. M., Kaastra J. S., Branduardi-Raymont G., Steenbrugge K. C., 2003, *Astrophys. J.*, **598**, 232
- Berkowitz J., 1979, *Photoabsorption, Photoionization and Photoelectron Spectroscopy*. Academic Press, New York, USA
- Berrington K., Quigley L., Zhang H. L., 1997, *J. Phys. B: At. Mol. & Phys.*, **30**, 5409
- Bingcong G., Wensheng D., 2000, *Phys. Rev. A*, **62**, 032705
- Bizau J.-M., Cubaynes D., Guilbaud S., Al Shorman M. M., Gharaibeh M. F., Ababneh I. Q., Blancard C., McLaughlin B. M., 2015, *Phys. Rev. A*, **92**, 023401
- Bizau J. M., et al., 2016, *J. Elec. Spec. Relat. Phenom.*, **210**, 5
- Blustin A. J., Branduardi-Raymont G., Behar E., Kaastra J. S., Kahn S. M., Page M. J., Sako M., Steenbrugge K. C., 2002, *Astron. and Astrophys.*, **392**, 453
- Blustin A. J., et al., 2003, *Astron. and Astrophys.*, **403**, 481
- Bruch R., Schneider D., Schwarz W. H. E., Meinhart M., Johnson B. M., Taulberg K., 1979, *Phys. Rev. A*, **19**, 587
- Bruch R., Stolerfohr N., Datz S., Miller P. D., Pepmiller P. L., Yamazaki Y., Krause H. F., Swenson J. K., 1987, *Phys. Rev. A*, **35**, 4114
- Burke P. G., 2011, *R-Matrix Theory of Atomic Collisions: Application to Atomic, Molecular and Optical Processes*. Springer, New York, USA
- Cabot S. H. C., Wang Q. D., Yao Y., 2013, *Mon. Not. Roy. Ast. Soc.*, **431**, 511
- Cassinelli J. P., Waldron W. L., Sanders W. T., Harnden Jr F. R., Rosner R., Vaiana G. S., 1981, *Astrophys. J.*, **250**, 677
- Chen M. H., 1985, *Phys. Rev. A*, **35**, 4579
- Chen M. H., 1986, *At. Data Nucl. Data Tables*, **34**, 301
- Chen M. H., Crasemann B., 1987a, *Phys. Rev. A*, **35**, 4579
- Chen M. H., Crasemann B., 1987b, *At. Data Nucl. Data Tables*, **37**, 419
- Chen F., Zhang M., Gou B., 2006, *J. Phys. B: At. Mol. Opt. Phys.*, **39**, 4249
- Davis B. F., Chung K., 1985, *Phys. Rev. A*, **31**, 3017
- Davis B. F., Chung K. T., 1989, *Phys. Rev. A*, **39**, 3942
- Fano U., Cooper J. W., 1968, *Rev. Mod. Phys.*, **40**, 441
- Ferland G. J., 2003, *Ann. Rev. of Astron. Astrophys.*, **41**, 517
- Ferland G. J., Korista K. T., Verner D. A., Ferguson J. W., Kingdon J. B., Verner E. M., 1998, *Pub. Astron. Soc. Pac. (PASP)*, **110**, 761
- Foster A. R., Ji L., Smith R. K., Brickhouse N. S., 2012, *Astrophys. J.*, **756**, 128
- Gabriel A. H., 1972, *Mon. Not. Roy. Astron. Soc.*, **160**, 99
- Garcia J., Mendoza C., Bautista M. A., Gorczyca T. W., Kallman T. R., Palmeri P., 2005, *Astrophys. J.*, **779**, 78
- Gatuzz E., et al., 2013a, *Astrophys. J.*, **768**, 60
- Gatuzz E., et al., 2013b, *Astrophys. J.*, **778**, 83
- Gatuzz E., Garcia J., Mendoza C., Kallman T. R., Bautista M. A., Gorczyca T. W., 2014, *Astrophys. J.*, **790**, 131
- Gorczyca T. W., et al., 2013, *Astrophys. J.*, **779**, 78
- Gu M. F., Schmidt M., Biersdorfer P., Chen H., Thorn D. B., Träbert E., Behar E., Kahn S. M., 2005, *Astrophys. J.*, **627**, 1066
- Gupta A., Mathur S., Krongold Y., Nicastro F., Galeazzi M., 2012, *Astrophys. J.*, 597, L8
- Gupta A., Mathur S., Galeazzi M., Krongold Y., 2014, *Astrophys. Space Sci.*, 352, 775
- Hibbert A., 1975, *Comput. Phys. Commun.*, **9**, 141
- Hitchcock A. P., Brion C. E., 1980, *J. Elec. Spec. Relat. Phenom.*, **18**, 1
- Hoffmann G., Müller A., Tinschert K., Salzborn E., 1990, *Z. Phys. D - Atoms, Molecules and Clusters*, **16**, 113
- Hoffmann G., Müller A., Weissbecker K., Stenke M., Tinschert K., Salzborn E., 1991, *Z. Phys. D - Atoms, Molecules and Clusters*, **21**, S189
- Juett A. M., Schulz N. S., Chakrabarty D., 2004, *Astrophys. J.*, **612**, 308
- Kaastra J. S., Steenbrugge K., Raassen A. J. J., van der Meer R. L. J., Brinkman A. C., Liedahl D. A., Behar E., de Rosa A., 2002, *Astron. and Astrophys.*, **386**, 427
- Kaastra J. S., et al., 2004, *Astron. and Astrophys.*, **428**, 57
- Kallman T. R., 2016, , private communication
- Kallman T. R., Bautista M. A., 2001, *Astrophys. J. Suppl. Ser.*, **134**, 139
- Kjeldsen H., Kristensen B., Brooks R. L., Folkman H., Knudsen H., Andersen T., 2002, *Astrophys. J. Suppl. Ser.*, **138**, 219
- Krongold Y., Nicastro F., Brickhouse N. S., Elvis M., Liedahl D. A., Mathur S., 2003, *Astrophys. J.*, 597, 832
- Lee J. C., Ogle P. M., Canizares C. R., Marshall H., Schulz N. S., Morales R., Fabian A. C., Iwasawa K., 2001, *Astrophys. J.*, **554**, L13
- Liao J. Y., Zhang S.-N., Yao Y., 2013, *Astrophys. J.*, **774**, 116
- Lin H., Hsue C.-S., Chung K. T., 2001, *Phys. Rev. A*, **65**, 032706
- McLaughlin B. M., Ballance C. P., 2015, in Resch M. M., Kovalenko Y., Fotch E., Bez W., Kobaysah H., eds., , *Sustained Simulated Performance 2014*. Springer, Berlin, Germany, pp 173–190
- McLaughlin B. M., Ballance C. P., Bowen K. P., Gardenghi D. J., Stolte W. C., 2013a, *Astrophys. J.*, **771**, L8
- McLaughlin B. M., Ballance C. P., Bowen K. P., Gardenghi D. J., Stolte W. C., 2013b, *Astrophys. J.*, **779**, L31
- McLaughlin B. M., Bizau J.-M., Cubaynes D., Al Shorman M. M., Guilbaud S., Sakho I., Blancard C., Gharaibeh M. F., 2014, *J. Phys. B: At. Mol. Opt. Phys.*, **47**, 065201
- McLaughlin B. M., Ballance C. P., Pindzola M. S., Müller A., 2015, in Nagel W. E., Kröner D. H., Resch M. M., eds., , *High Performance Computing in Science and Engineering'14*. Springer, Berlin, Germany, pp 23–40
- McLaughlin B. M., Ballance C. P., Pindzola M. S., Schippers S., Müller A., 2016, in Nagel W. E., Kröner D. H., Resch M. M., eds., , *High Performance Computing in Science and Engineering'15*. Springer, Berlin, Germany, pp 51–74
- McLaughlin B. M., Ballance C. P., Pindzola M. S., Stancil P. C., Schippers S., Müller A., 2017, in Nagel W. E., Kröner D. H., Resch M. M., eds., , *High Performance Computing in Science and Engineering'16*. Springer, Berlin, Germany, p. submitted for publication
- Mendoza C., et al., 2012, *The Reliability of atomic data used for oxygen abundance determinations*, Conference on Mapping Oxygen in the Universe, Instituto de Astrofísica de Canarias, May 14–18, <http://www.iac.es/congreso/oxygenmap/media/presentations/>
- Miller M. J., Bergman J. N., 2015, *Astrophys. J.*, 800, 14
- Mitnik D. M., Pindzola M. S., Griffin D. C., Badnell N. R., 1999, *J. Phys. B: At. Mol. Opt. & Phys.*, **32**, L479
- Moore C. E., 1993, in Gallagher J. W., ed., , *CRC Series in Evaluated Data in Atomic Physics*. CRC Press, Boca Raton, FL, p. 399
- Müller A., 2015, *Phys. Scr.*, **5**, 054004
- Müller A., et al., 2009, *J. Phys. B: At. Mol. Opt. Phys.*, **42**, 235602
- Müller A., et al., 2010, *J. Phys. B: At. Mol. Opt. Phys.*, **43**, 135602
- Müller A., et al., 2014, *J. Phys. B: At. Mol. Opt. Phys.*, **47**, 135201
- Murakami I., Safronova U. I., Kato T., 2002, *Can. J. Phys.*, **80**, 1525
- Nahar S. N., Pradhan A. K., Zhang H. L., 2001, *Phys. Rev. A*, **63**, 060701(R)
- Nicastro F., Senatore F., Gupta A., Guainazzi M., Mathur S., Krongold Y., Elvis M., Piro L., 2016a, *Mon. Not. Roy. Astro. Soc.*, **457**, 676
- Nicastro F., Senatore F., Gupta A., Guainazzi M., Mathur S.,

- Krongold Y., Elvis M., Piro L., 2016b, *Mon. Not. Roy. Astro. Soc.*, **458**, L123
- Nicastro F., Senatore F., Krongold Y., Elvis M., 2016c, *Astrophys. J.*, **828**, L12
- Nicolosi P., Tondello G., 1997, *J. Opt. Soc. Am.*, **67**, 1033
- Ogle P. M., Mason K. O., Page M. J., Salvi N. J., Cordova F. A., McHardy I. M., Priedhorsky W. C., 2004, *Astrophys. J.*, **606**, 151
- Petrini D., Tully J. A., 1991, *Astron. Astrophys.*, **241**, 327
- Piingos N. A., Nicolaides A., 1993, *Phys. Rev. A*, **48**, 4142
- Pinto C., Kaastra J. S., Costantini E., de Vries C., 2013, *Astron. and Astrophys.*, **551**, 25
- Pinto C., Costantini E., Fabian A. C., Kaastra J. S., in'tZand J. J. M., 2014, *Astron. and Astrophys.*, **563**, A115
- Pradhan A. K., 2000, *Astrophys. J.*, **545**, L165
- Pradhan A. K., Chen G. X., Delahaye F., Nahar S. N., Oelgoetz J., 2003, *Mon. Not. R. Astron. Soc.*, **341**, 1268
- Ramírez J., 2013, *Astron. and Astrophys.*, **551**, A95
- Robicheaux F., Gorczyca T. W., Griffin D. C., Pindzola M. S., Badnell N. R., 1995, *Phys. Rev. A*, **52**, 1319
- Sakho I., 2011, *Rad. Phys. Chem.*, **80**, 1295
- Sakho I., 2012, *Phys. Rev. A*, **86**, 052511
- Sakho I., Diop B., Faye M., Sène A., Gueye M., Ndao A. S., Biaye M. Wagué A., 2013, *At. Data. Nucl. Data Tables*, **99**, 447
- Samson J. A. R., 1967, *Techniques of Vacuum Ultraviolet Spectroscopy*. John Wiley & Sons, New York, USA
- Schmidt M., Biersdorfer P., Chen H., Thorn D. B., Träbert E., Behar E., 2004, *Astrophys. J.*, **627**, 1066
- Scully S. W. J., et al., 2005, *J. Phys. B: At. Mol. Opt. Phys.*, **38**, 1967
- Shore B. W., 1967, *Rev. Mod. Phys.*, **39**, 439
- Tanaka T., et al., 2008, *Phys. Rev. A*, **78**, 022516
- West J., 2001, *J. Phys. B: At. Mol. Opt. Phys.*, **34**, R45
- Wu L.-J., Xi J.-H., 1991, *J. Phys. B: At. Mol. Phys.*, **24**, 3351
- Yao Y., Shultz N. S., Gu M. F., Nowak M. A., Canizares C. R., 2009, *Astrophys. J.*, **696**, 1418
- Zhang S. B., Yeager D. L., 2012a, *J. Mol. Structure*, **1023**, 96
- Zhang S. B., Yeager D. L., 2012b, *Phys. Rev. A*, **85**, 032515

This paper has been typeset from a \LaTeX file prepared by the author.